



## Comparative Study of Properties of TiO<sub>2</sub> Prepared by Reactive Sputtering and Sol-gel method

**Yas Khudair  
Ahmed Hassan**

Al-Karkh University Science of College / Department of Medical Physics/ yas127752@gmail.com

**Zahraa Ibrahim Yossef Oraibi**

Elm City University College  
Department Medical physics /zi337431@gmail.com

**Douha Auday lafta kareem**

Almustaqbal univercity college Department Medical physics /huu19998@gmail.com

**Zeina Ismail Abd Hassan**

Hilla University College Department Applied medical physics / zeenayaqot@gmail.com

**Karima abdali mhana  
hamad**

wasit university Science of College Department medical physics / kkr4480@gmail.com

ABSTRACT

Nanostructured Titanium dioxide were synthesized using two different deposition techniques: sol-gel and sputtering. Anatase structural phase of titania was observed for the samples synthesized by both methods by controlling temperture. The scanning electron microscopy indicated that the average particle size of samples prepared by plasma sputtering was smaller than that of samples prepared sol-gel. The spectroscopic measurements confirmed the formation of Ti-O bonds. Energy band gap was determined and found to be 3.2 eV for sample prepared by sol-gel and 3.1 eV for samples prepared by plasma sputtering. These results highlight the advantages of plasma sputtering technique over sol-gel as thin film deposition methods.

**Keywords:**

Nanostructured Titanium dioxide, sol-gel and sputtering

## Introduction

Titanium Dioxide ( $\text{TiO}_2$ ) is widely regarded as one of the most versatile and valuable materials in the realm of advanced materials science. It exhibits remarkable properties such as high refractive index, strong UV light absorption, and resistance to chemical and biological degradation. These characteristics render it indispensable in a variety of applications, including photocatalysis, solar energy conversion, and as a pigment in paints and coatings. Moreover,  $\text{TiO}_2$  is used in the manufacturing of cosmetics and sunscreens due to its ability to protect skin from ultraviolet light.

Among the various methods of synthesis, reactive sputtering and the sol-gel method have gained prominence due to their unique advantages and the distinct properties they impart to the  $\text{TiO}_2$  produced. Reactive sputtering is a physical vapor deposition (PVD) technique that involves the ejecting of material from a 'target' source onto a substrate in the presence of a reactive gas, such as oxygen. This method is highly favored in applications requiring thin films of  $\text{TiO}_2$  with high density and uniformity. The ability to control film thickness and stoichiometry precisely through reactive sputtering is critical for applications in photovoltaic devices and sensors. Furthermore, the reactive sputtering process can be finely tuned to alter the crystal structure of  $\text{TiO}_2$ , thereby enabling the enhancement of its photocatalytic activity and optical properties. On the other hand, the sol-gel method is a chemical synthesis route that involves the transition of a system from a liquid 'sol' into a solid 'gel' phase.[1]

Comparative studies of  $\text{TiO}_2$  synthesized by different methods are essential to understand how the synthesis influences the properties and suitability of  $\text{TiO}_2$  for specific applications. By comparing the physical, chemical of  $\text{TiO}_2$  prepared via reactive sputtering and the sol-gel method and determine which method is more suitable for photocatalytic efficiency.[2]

### 1-1 Titanium dioxide ( $\text{TiO}_2$ ):

Titanium dioxide, also known as titania, is the inorganic compound with the chemical formula  $\text{TiO}_2$ . It was discovered in 1821 and is considered to be one of the top 20 inorganic chemicals of industrial importance [3].  $\text{TiO}_2$  has been demonstrated to be an appropriate photocatalyst among the many semiconductor photocatalysts employed due to its thermal stability, insolubility in water, chemical inertness, and non-toxicity.  $\text{TiO}_2$  is widely used in industrial applications such as photocatalyst, paints, printing inks, cosmetics, ceramics and also in the pharmaceutical sector [4]. Titanium is the fourth most abundant element and the ninth most abundant metal in the earth's crust (~63%). Titanium dioxide is found bound in minerals such as ilmenite (titanium iron oxide) and perovskite (calcium titanium oxide), as well as in purer mineral forms such as anatase, brookite, and rutile [5].

### 1-2 Crystalline structure of $\text{TiO}_2$ :

Titanium dioxide, has three crystal phases anatase, rutile, and brookite.  $\text{TiO}_2$  has a temperature-dependent composition; at calcination temperatures of more than 500 K, the anatase phase is converted to rutile [6]. In all three of its main dioxides, titanium exhibits octahedral geometry, being bonded to six oxide anions. The

oxides in turn are bonded to three Ti centers. Although rutile is the more thermodynamically stable phase of  $\text{TiO}_2$  at all temperatures [7], anatase is usually the first phase generated in many synthesis techniques due to the less limited structural rearrangement required to form this phase from an amorphous phase [8]. Anatase and rutile are both tetragonal in structure, while the brookite structure is orthorhombic. Each octahedron in the rutile structure is in connection with ten neighboring octahedrons (two sharing edge oxygen pairs and eight sharing corner oxygen atoms), whereas each octahedron in the anatase structure is in contact with eight neighbors (4 sharing an edge and four sharing a corner). In Brookite, the octahedral connection is such that three edges per octahedron are shared [9].

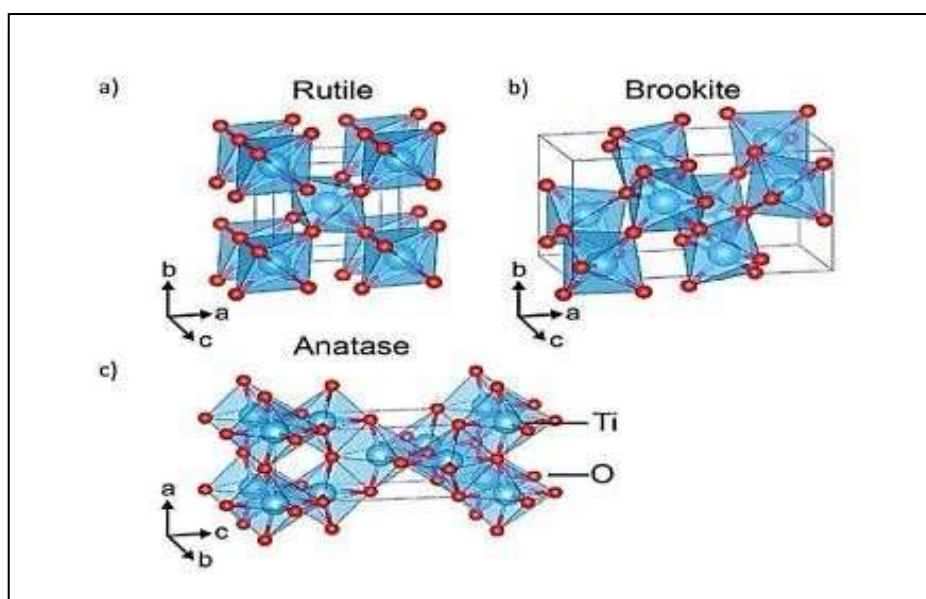


Figure (1-1):  $\text{TiO}_2$  crystal structures: (a) Rutile, (b) Brookite, and (c) Anatase

### 1-3 Sputtering Mechanism:

The sputtering process can be occurring by applying an electric field from an outside power source, charging the target with

high negative voltage (3 to 5 kV). A gas is inserted into the vacuum chamber between the target and chamber wall and the substrate. The large potential difference causes the ionization of introduced gas in the high electric field that forms plasma [10]. The ionization results in a negatively charged electron and positively charged ion pairs, whereas the plasma itself retains net neutral charge. Positively charged ions are attracted to the negatively charged target and accelerated by electric field, resulting in a collision with the target material. When an ion approaches the surface of a target, one or the entire following phenomenon may occur (figure 1-2) [11]. Many of these events that occur during sputter deposition are not desired, and may be considered losses in energy. A term, known as the sputter yield, is used to quantify the effectiveness of sputtering. The sputter yield is defined as the number of atoms sputtered from a target surface per incident ion. The sputter yield can be optimized by considering the kinetic energy of ions and the momentum exchange between ions and target atoms. The kinetic energy of the impacting ion needs to be large enough to overcome the binding energy of the target atoms to successfully sputter target atoms [12]. At too low of energy, the ion will not have enough energy to sputter, and will likely be reflected from the target surface as either a neutral or ion. The impact of the ion may cause the target to eject an electron, usually referred to as a secondary electron. At too high of energy, the ion will bury into the target surface. This is the phenomenon of ion implantation. The ion impact may also be responsible for some

structural rearrangements in the target material. The ion impact may set up a series of collisions between atoms of the target, possibly leading to the ejection of one of the neutral atoms from the

material by momentum transfer. The ejection process is known as sputtering. The sputtered atoms leave the target surface towards the substrate where they condense and form a thin film [13].

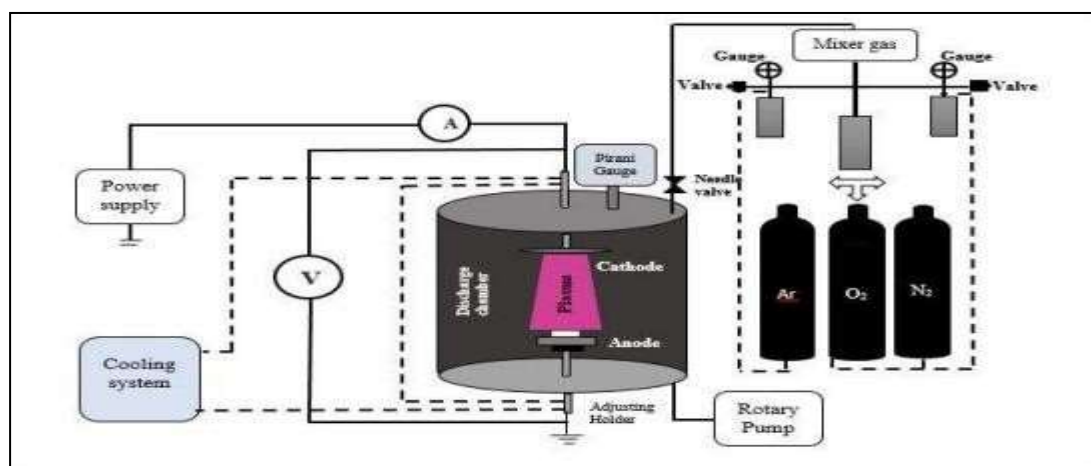


*Figure (1-2) Sketch of the sputter deposition setup*

Sputtering technique, it became one of the most important technologies for preparing thin films of almost any material. Some of the main advantages of sputtering are good adhesion to the substrate, excellent uniformity on large-area substrates, ability of the deposit to maintain stoichiometry of the original target composition, ease of controlling film thickness, relatively cheap deposition method, film generation speeds are stable and similar in various different materials, films for various materials such as metal, alloy, compound and insulating materials and oxide and nitride film can be generated through reactive sputter of  $O_2$  and  $N_2$ . And the Disadvantages of sputtering are film inequality and damage are caused by high energy deposition after film generation, inequality and damage can be reduced by thermal treatment, film is heated by the exposure to electron, ion, etc. ( $100\sim 150^\circ C$ ) and film generation condition is sensitive and gives an effect to each other it is necessary to adjust sputtering parameters [15].

#### 1-4 Reactive Magnetron Sputtering:

In reactive sputtering, compound thin films are deposited by sputtering from metal, alloy or compound targets in the presence of a reactive gas. The reactive gas reacts with the sputtered material and forms a compound (e.g. an oxide when the reactive gas is oxygen). This makes it possible to deposit a wide variety of compounds (oxides, nitrides, carbides, etc.) with a wide range of properties [16]. This versatility gives reactive sputtering a distinct advantage and is one of the reasons for its frequent use in industrial applications.

Figure (1-3) is an illustration of the reactive sputtering process. Thin film properties are strongly dependent on the composition of the deposited film. Hence, there are great interests in being able to control the film composition. The most straightforward way is to adjust the reactive gas flow.

Simply, a higher reactive gas flow to the system gives a higher concentration in the film. However, the relationship between the reactive gas flow and film composition is normally very highly complex.

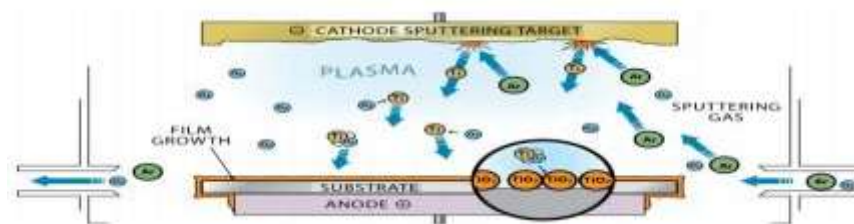


Figure (1-3) Illustration of the reactive sputtering process

When introducing a reactive gas like oxygen or nitrogen, the reactive gas atoms will react with the sputtered target atoms and form a compound film at all surfaces in the chamber, including at the target surface. However, compound formation at the target (poisoning) normally causes the sputtering rate to drop [17]. The concentration of reactive gas in the film is normally quenched at a certain flow of gas. The reactive gas concentration corresponds to the stoichiometric composition of the compound. Increasing the reactive gas flow further will not change the composition but decrease the deposition rate. Since a reduction in deposition rate is highly undesirable, the optimum processing point is where the supply of reactive gas is precisely sufficient for obtaining stoichiometric films [18].

#### 1-5 Sol-gel process:

The sol-gel process, as the name implies, involves transition from a liquid “sol” (colloidal solution) into a “gel” phase. Usually

inorganic metal salts or metal organic compounds such as metal alkoxide are used as precursors. A colloidal suspension or a “sol” is formed after a series of hydrolysis and condensation reaction of the precursors. Then the sol particles condense into a continuous liquid phase (gel) [19]. Generally, three reactions are used to describe the sol-gel process: hydrolysis, alcohol condensation and water condensation. Because water and alkoxides are immiscible, alcohol is commonly used as co-solvent. The two phases which describe the sol-gel process are defined as follows [20]:

Sol: a stable suspension of colloidal solid particles or polymers in a liquid.

Gel: porous, three-dimensional, continuous solid network surrounding a continuous liquid phase.

Typically, a sol-gel process is based on five processing steps(Fendler, 2008).

- i. Hydrolysis of alkoxide precursors which forms a polymeric or particulate sol containing inorganic materials.
- ii. Formation of a uniform suspension by deposition of substrate into the sol.
- iii. Solidification of the gel with solvent and volatile compounds evaporation process.
- iv. Drying at room temperature to get a condensed inorganic network.
- v. Calcination where very high temperature is involved to remove of organics and to crystallize the solid material.

#### 2-1 Introduction:

In this chapter, the experimental parts of the work are presented. It includes synthesis titanium dioxide nanostructure by magnetron sputtering technique, optical and structural measurements.

#### 2-2 Sputtering System:

The lab-made magnetron sputtering system used in this work involves the following parts: vacuum chamber discharge electrodes and magnetron assembly, vacuum unit, dc power supplies, gas mixer chamber and measuring equipment. The system is described schematically in figure (2-1).



*Figure (2-1) Schematic representation of the system presented in this work*

### 2-2-1 Vacuum Chamber:

A vacuum deposition chamber is a cylindrical made up of two open ends, made from stainless steel. The two open ends are closed

with two stainless steel flanges of 45 cm in diameter. The lower end contains a feedthrough for electrical connections required for experiment. The upper end contained two feedthroughs; one for the gas inlet and Pirani gauge and the other for the Penning gauge. Both flanges include a central hole for the electrode hollow holder. Rubber O-rings act as a vacuum sealant between the feed-through and the chamber and silicon vacuum grease is used at all sealing points. The chamber has an internal diameter of 35 cm, an outer diameter of 45 cm, and a height of 37.5 cm. The chamber includes four side windows to monitor the events of plasma inside.

### 2-2-2 Discharge Electrodes and Magnetron Assembly:

It was decided to use stainless steel for the anode and cathode electrodes of the discharge. The cathode is made up of hollow disks with a diameter of 80 mm and a thickness of 8.5 mm. The anode is an 80 mm in diameter and 6.5 mm thick disk. The anode might be heated to 350°C using a controlled heating system. Two permanent ring magnets were positioned on the cathode's backside to form the magnetron.

### 2-2-3 Vacuum Unit:

The chamber was evacuated by a rotary pump to reach a vacuum pressure of about  $10^{-2}$  mbar inside the chamber. One gauge was utilized to determine the pressure inside the chamber; the low pressure of  $10^{-2}$  mbar, measured using an Edward Pirani gauge.

### 2-2-4 Gas Supply System and Gas Mixing Unit:

The gas mixer was made from stainless steel in this system and it contains two cylinders to mix argon and oxygen gases. The gauges have been placed on the top of two cylinders, which each include a highly accurate valve for ideal gas mixing.

### *2-2-5 DC Power Supply:*

The required electrical power for generating discharge inside the vacuum chamber was provided by a 5 kV dc power supply. A current-limiting resistance was connected between the negative terminal of the DC power supply and the cathode, while the positive terminal of the DC power supply was connected directly to the anode. The output voltage of the power supply could be varied precisely over 0-5 kV to control the current flowing between discharge electrodes.

### *2-3 Sputtering Targets and Substrates:*

The target for sputtering was titanium sheet of 99.99% purity used as the electrodes. Ti sheet 8 cm in diameter and 0.5 mm thick. Highly-pure oxygen gas was used as the reactive gas required for the TiO<sub>2</sub> samples to be prepared.

The transparent substrates used in this work were made of substrate glass. The surfaces of the samples were cleaned with ethanol to remove any oil layers or residuals that may have formed on their surfaces, rinsed and washed with distilled water to remove the ethanol, and then dried completely before being placed in a vacuum chamber for sputtering experiments

### *2-4 Operating Conditions:*

Vacuum pressure, inter-electrode spacing, discharge voltage, discharge current, and deposition time are all constant operating conditions. In addition, the gas mixing ratio (Ar:O<sub>2</sub>) was changed to study the influence on the prepared samples. The figure shows the processes of ejecting titanium atoms from the target and directing them towards the slide.

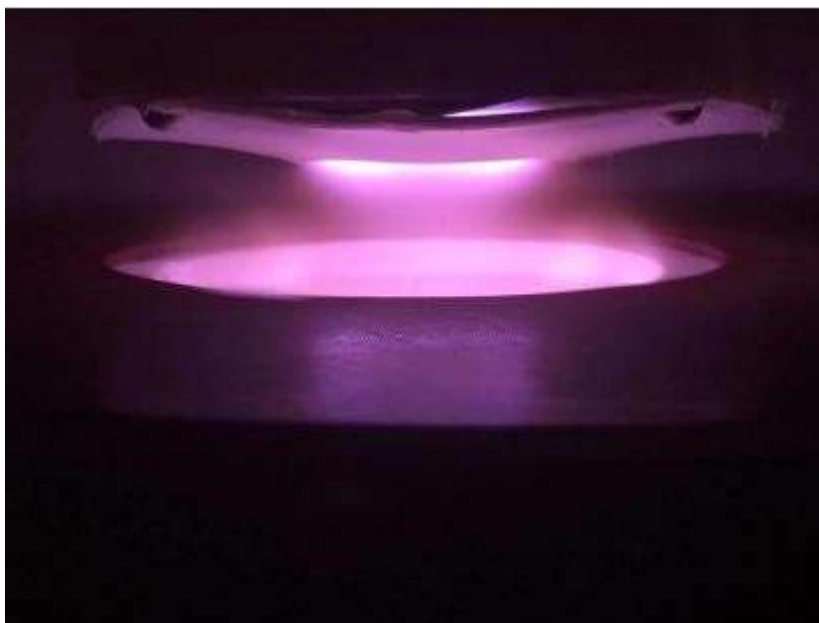


*Figure (2-2) Photographs of discharge plasma generated between the two electrodes at optimum operating conditions*

#### 2-5 Synthesis of TiO<sub>2</sub> thin films:

Titania films were prepared by the sputtering system of 99.9% purity titanium (Ti) sheet with a diameter of 8 cm. The chamber of the system is evacuated by a rotary vacuum pump to a base pressure of about  $8.5 \times 10^{-2}$  mbar. After that, the gas mixture is allowed to flow from the gas mixing unit into the chamber through a needle valve to keep the pressure of the gas mixture constant inside the deposition chamber. Oxygen was used as a reactive gas, and argon was used as

a sputtered gas. The pressure of oxygen gas should be relatively low to avoid the situation of target poisoning. Many parameters could be used to control the operation and sputtering processes in this work. The variable parameter is the mixing ratio of precursor gas (Ar) and reactive gas (O<sub>2</sub>). This plays a very important role in finalizing the deposition process and the appearance of thin films. The gas mixing ratio (Ar:O<sub>2</sub>) was varied as (50:50) and (70:30).

While the constant parameters include discharge voltage, discharge current, base pressure in the chamber, inter-electrode distance 4 cm and deposition time.

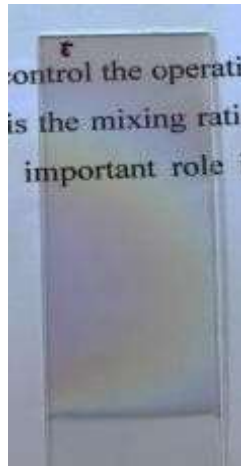


Figure (2-3) Photograph of  $\text{TiO}_2$  thin film

#### 2-6 Measurements and Characterization:

Different measurements were carried out on the prepared  $\text{TiO}_2$  samples they include thickness measurements, x-ray diffraction (XRD) patterns, Fourier-transform infrared (FT-IR), scanning electron microscopy (SEM) and UV-Visible spectroscopy.

##### 2-6-1 Determination of Film Thickness:

The thickness of thin films was determined using the Tolansky method, which employed a diode laser (632.8 nm) with a  $45^\circ$  incidence angle, as schematically depicted in Figure (2-4). This method is based on the interference between the laser beam reflected

from the thin film surface and the substrate, and the film thickness

(t) was estimated using the formula below [21]

$$t = \frac{\lambda}{2x_2} x_1$$

Where  $x_1$  is the fringe width,  $x_2$  is the distance between two fringes and  $\lambda$  is the wavelength of laser light.

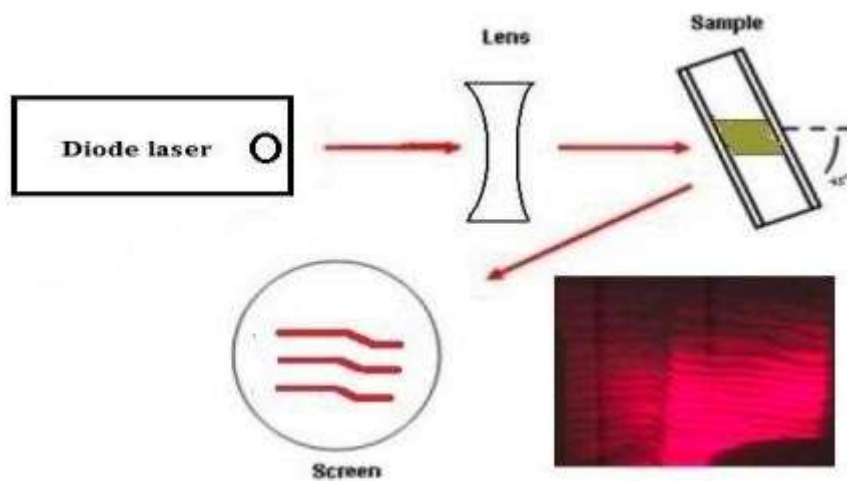


Figure (2-4) shows a schematic diagram of the film thickness measurement

2-6-2 X-ray diffraction (XRD):

The structures of the prepared samples were analyzed with XRD system (Cu-K $\alpha$  x-ray tube with  $\lambda=1.54056 \text{ \AA}$ ). A proportional counter of 40 kV and current of 30 mA was used. The XRD patterns were recorded  $2\theta$  ranges of 20-80 $^\circ$ .

### 2-6-3 Fourier-Transform Infrared Spectroscopy (FTIR):

Fourier-transform Infrared (FTIR) spectrometry was carried out by a SHIMADZU FTIR-8400S spectrophotometer to determine the structure of prepared samples.

### 2-6-4 Scanning Electron Microscopy (SEM):

The scanning electron microscopy was performed on the prepared samples using) was used with the samples prepared at the optimum conditions were studied in order to confirm the formation of nanostructures as well as introduce the effects of some operation conditions on the fine structures of the prepared samples.

### 2-6-5 Ultraviolet-Visible Spectroscopy (UV-Vis):

Ultraviolet-Visible Spectroscopy (UV-Vis) measures the amount of absorption of spectroscopy within a specific region of ultraviolet and visible radiation. The spectrophotometer is composed of three parts: the light source, the dispersive, and the detector. A sample is put between a light source and a photodetector, where the strength of a UV-Vis light beam is measured before and after the sample passes through. UV-Vis absorption spectroscopy depends on

the measurement of the percentage of absorbed radiation at each wavelength. Usually, it is performed by scanning the specimen via a

range of wavelengths and recording absorption. The energy bandgap was calculated from the following equation [22]:

$$E_g = \frac{1240}{\lambda} \text{ eV}$$

(2-2)

Where  $E_g$  is the energy band gap in electron volts (eV), can be calculated from the absorption and transmission spectrum measured, and  $\lambda$  is the wavelength in nanometers of the absorption edges in the spectrum (nm).

## 3-1 Introduction:

In this chapter, the characterizations and optical of the prepared samples were determined by different tests, such as X-ray diffraction (XRD) patterns, Fourier-Transform Infrared (FTIR) scanning electron microscopy (SEM) and UV-VIS. Spectroscopic measurements.

### 3-2 X-ray Diffraction Measurement:

The XRD pattern of  $\text{TiO}_2$  thin film prepared using gas mixing ratios of Ar: $\text{O}_2$  (50:50) by sputtering technique and  $\text{TiO}_2$  prepared using Sol-gel method as shown in figures (3-1), (3-2).

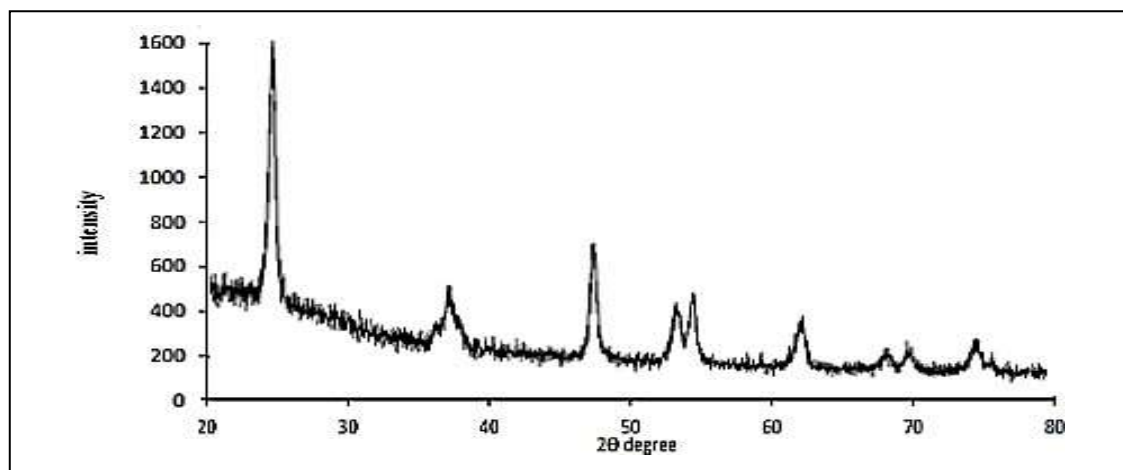


Figure (3-1) XRD pattern for  $\text{TiO}_2$  thin film prepared using sputtering technique

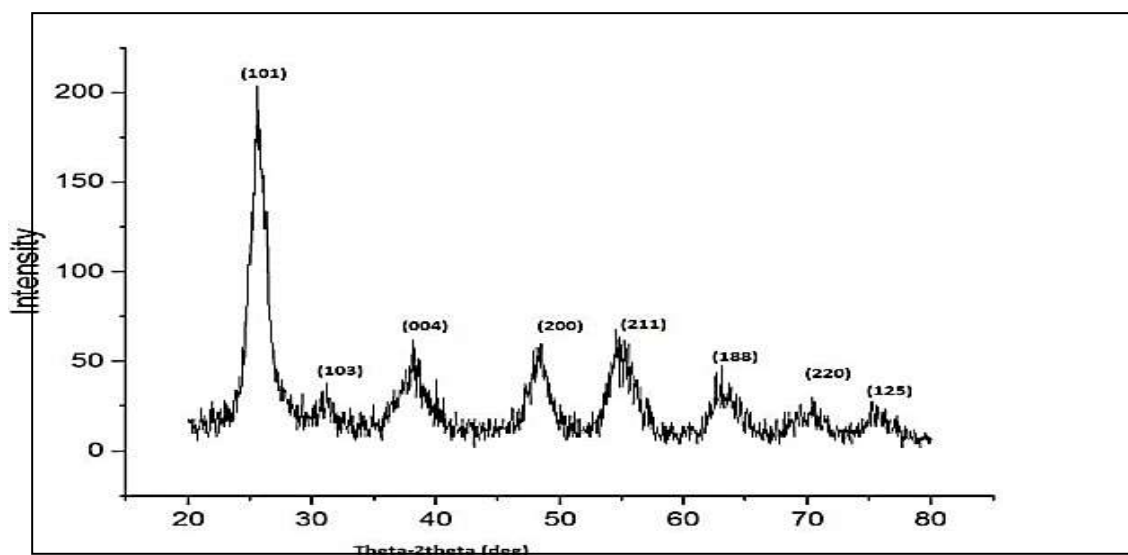


Figure (3-2) the X-Ray diffraction pattern of  $\text{TiO}_2$  prepared by sol-gel technique

As shown in this figures, the peaks are clearly observed and they all assigned to the anatase crystalline phase of  $\text{TiO}_2$  and agree with the JCPDS card No. 21-1272 (anatase  $\text{TiO}_2$ ). No peaks belonging to the rutile phase was found in the prepared sample, both the technique give the anatase phase of titania by controlling parameters of each technique

### 3-3 Fourier-Transform Infrared (FTIR) Spectroscopy:

FTIR analysis is used to determine the type of bonding established in a sample. The FTIR of  $\text{TiO}_2$  is presented in figures (3- 3), (3-4).

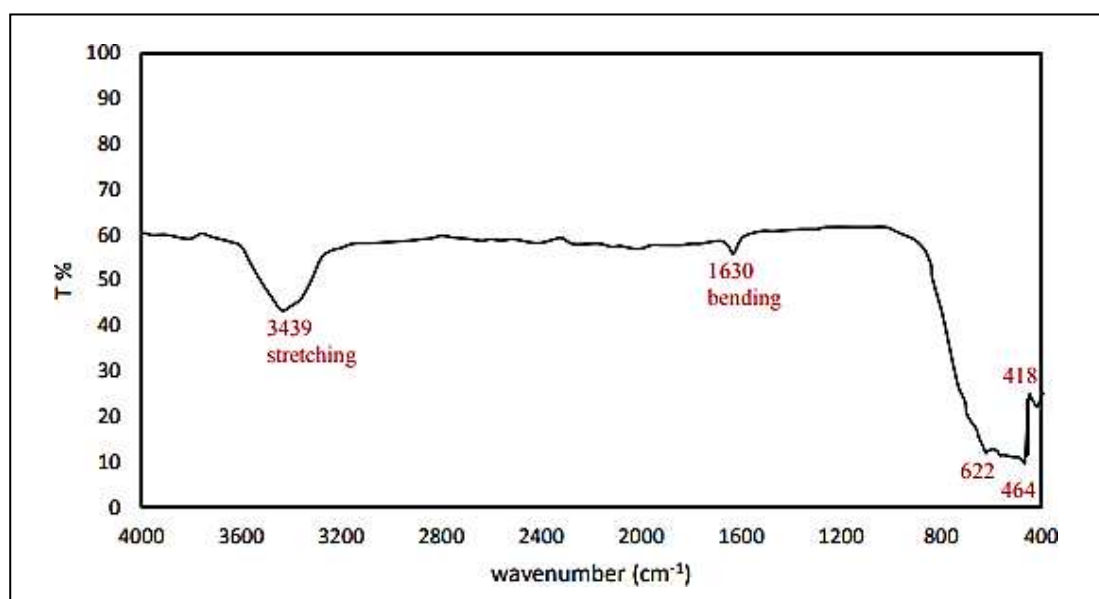


Figure (3-3) FTIR spectrum of  $\text{TiO}_2$  thin film prepared using sputtering technique

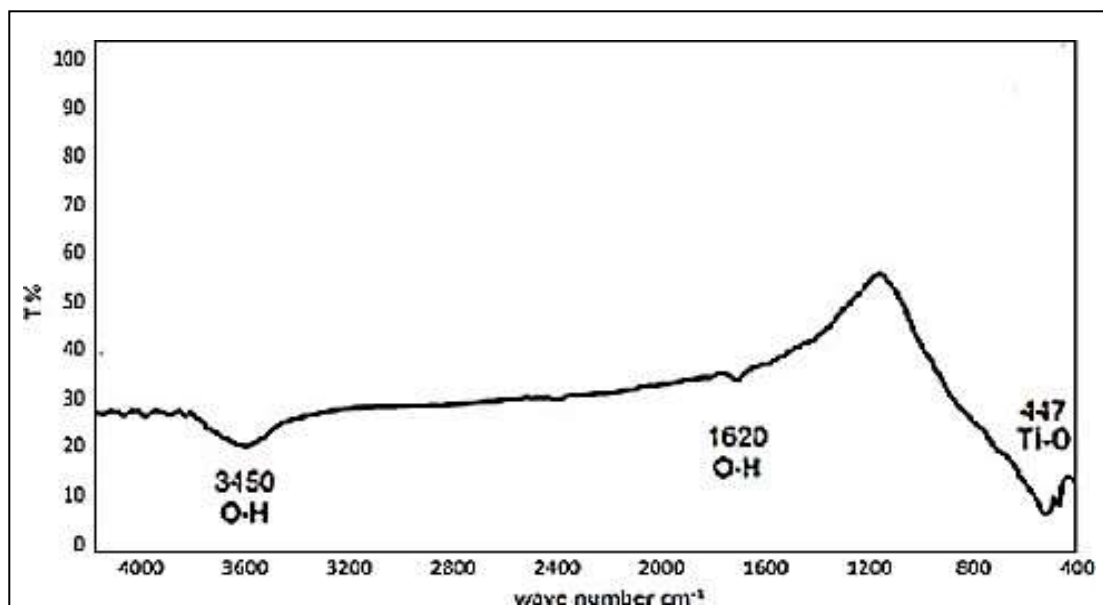


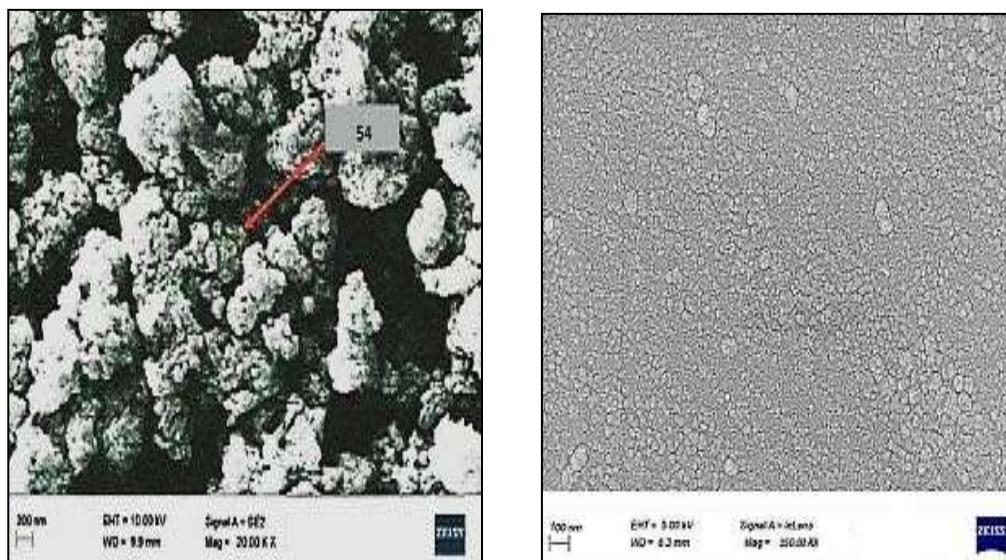
Figure (3-4) FTIR spectrum of TiO<sub>2</sub> thin film prepared using sol-gel

From figures the band assigned to Ti-O stretching vibration has been observed at around 447, 446 and 622 cm<sup>-1</sup> while the peak at 418 cm<sup>-1</sup> is ascribed to Ti-O-Ti bonds in the TiO<sub>2</sub> lattice. The peaks around 3450 and 1620 cm<sup>-1</sup> are attributed to the stretching

and bending vibration of the OH group in water molecules in atmosphere. The FTIR spectrum confirms the absence of any impurities in the prepared samples by both methods.

### 3-4 Scanning Electron Microscope:

SEM microscopy was used to determine the surface profile and particle size of the produced thin films (SEM).



(a)

(b)

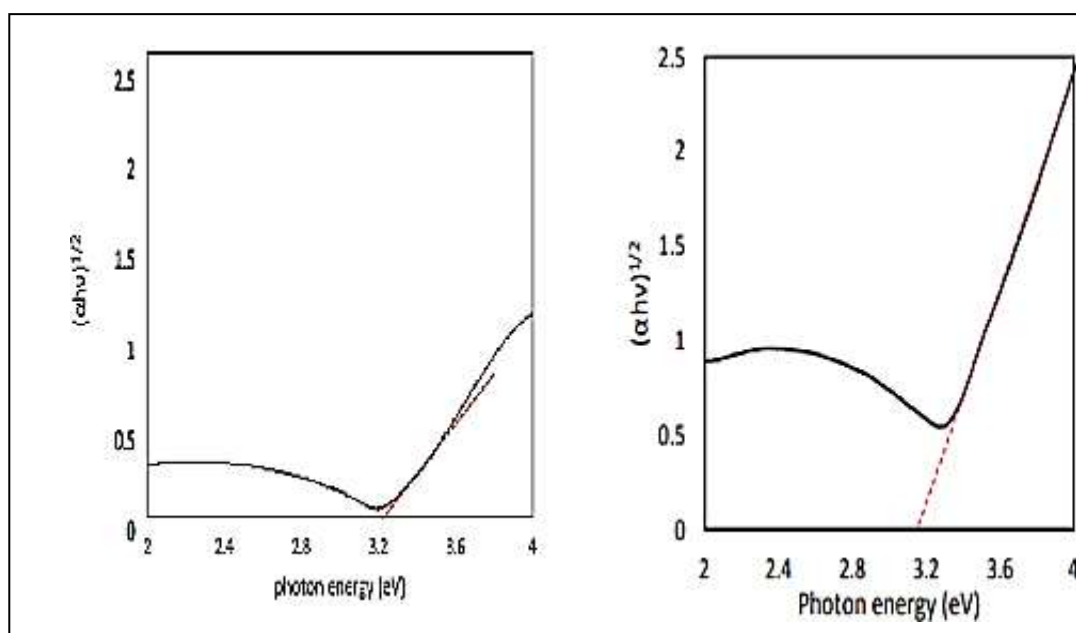
*Figure (3-4) SEM images of TiO<sub>2</sub> nanoparticles (a) Sol-gel (b) sputtering technique*

Figure (3-4) shows the SEM micrographs of the Titania samples prepared in this work by both methods. The SEM micrograph in Fig.

(a) shows Titania nanoparticles prepared by sol-gel method. It can be observed that the average particle size is 54 nm. Figure (b) shows Titania nanoparticles prepared by sputtering technique. The average particle size is 17.5 nm. This large difference in average particle size can be considered as an advantage of sputtering technique in

nanostructure fabrication. It also can be seen that the aggregation over the prepared nanoparticles is relatively low.

### 3-5 UV-VIS. Spectroscopic measurements:



Figures (3-5) Energy band gap ( $E_g$ ) of the  $TiO_2$  nanostructures prepared by sol-gel and sputtering technique

Using Tauc's equation, the band gap energy of prepared thinfilm samples can be determined as:

$$(\alpha h\nu)^{1/n} = A (h\nu - E_g)$$

where  $h$  is the Planck's constant,  $\nu$  is the photon frequency,  $E_g$  is the band gap energy, and  $A$  is a constant. The energy band gap was determined to be 3.15 eV for the sample prepared by sputtering and

3.2 eV for the sample prepared by sol-gel as shown in Figure (3-5).

### 3-6 Conclusion:

In concluding the structural and optical properties of the nanostructured titanium dioxide synthesized by sol-gel method and sputtering technique have been compared. Titanium dioxide nanostructures prepared in this work was same anatase phase in all two methods. little aggregation and higher homogeneity of nanoparticles prepared by

sputtering technique. The band gap energy of the film samples prepared by sputtering (3.15 eV) was lower than that prepared by sol-gel (3.2 eV). Accordingly, we can conclude that sputtering technique is better to synthesize TiO<sub>2</sub> due to high uniformity of film thickness, good control of deposition rate, good adhesion of film to substrate and good optical properties.

#### References:

1. Materials. (2018). Reactive sputtering for TiO<sub>2</sub> films.
2. IntechOpen. (n.d.). Sol-gel method for TiO<sub>2</sub>. Retrieved from
3. S. Riyas, V. A. Yasir and P. N. Mohan Das, "Crystal structure transformation of TiO<sub>2</sub> in presence of Fe<sub>2</sub>O<sub>3</sub> and NiO in air atmosphere", *Bulletin of Materials Science*, 25, p. 267–273, 2002.
4. A. R. Khataee and M. B. Kasiri, "Photocatalytic degradation of organic dyes in the presence of nanostructured titanium dioxide: influence of the chemical structure of dyes", *Journal of Molecular Catalysis A: Chemical*, 328, p. 8-26, 2010.
5. Carp, O., Huisman C. L. and Reller A., "Photoinduced reactivity of titanium dioxide", *Progress in Solid State Chemistry*, 32, p. 33-177, 2004.
6. RAB Devine, J-P Duraud, and E. Dooryh e, "Structure and Imperfections in Amorphous and Crystalline Silicon Dioxide", chemistry, 2000.
7. B. E. Warren, H. Krutter and O. Morningstar, "Fourier analysis of X-ray patterns of vitreous SiO<sub>2</sub> and B<sub>2</sub>O<sub>2</sub>", *Journal American Ceramic Society*, 19, 202, 1936.
8. C. R. Helms, "The Atomic and Electronic Structure of the Si- SiO<sub>2</sub> Interface," in *The Physics and Chemistry of SiO<sub>2</sub> and the Si-SiO<sub>2</sub> Interface*, New York: Plenum Press, p. 187, 1988.
9. N. Wiberg, A. Holleman and E. Wiberg, "Inorganic Chemistry", (Academic Press, 1st edition, 2001.
10. Richard Catlow, "Defects and disorders in crystalline and amorphous solids", Springer Netherlands, 418, p. 511, 1994.
11. Jean-Marie, "Composite Materials: mechanical behavior and Structural Analysis", Springer, p. 646, 1998. [66] William D. Callister Jr. and David G. Rethwisch, "Materials Science and Engineering: An Introduction", John Wiley & Sons, Inc., p. 992, 2018.

12. Tri-Dung Ngo, "Introduction to Composite Materials", intechopen, 91285, 2019.
13. Thornton, J.A. and Greene, J.E., "Sputter deposition processes", in Handbook of Deposition Technologies for Films and Coatings, p. 275-337, 1994.
14. B. Champman, "Glow discharge processes: Sputtering and Plasma etching", Wiley, New York, 1980.
15. K. Seshan, "Handbook of Thin-Film Deposition Processes and Techniques", Noyes Publications, New York, USA, 2002.
16. R. F. Bunshah, "Deposition technologies for films and coatings", Noyes Publications, New Jersey, 1994. [78] A. Rockett, "The material science of semiconductors", Springer, New York, 2008.
17. Laurette Combadiere, Jean Machet, "Reactive magnetron sputtering deposition of TiN films. I. Influence of the substrate temperature on structure, composition and morphology of the films", Surface and Coatings Technology, Vol. 88, pp. 17-27, 1997.
18. Diederik Depla, Zhaoyang Chen, Annemie Bogaerts, V. Ignatova, " Modeling of the target surface modification by reactive ion implantation during magnetron sputtering ", Journal of Vacuum Science & Technology A Vacuum Surfaces and Films, Vol. 22(4), pp.1524-1529, 2004.
19. M. Saraiva, "Sputter Deposition of MgO Thin Films: The Effect of Cation Substitution", PhD thesis, Universiteit Gent, Belgium, pp. 22-28, 2012.
20. L. Yang, Fabrication and characterization of microlasers by the Sol-Gel method", PhD Thesis, California institute of technology, Pasadena, California, USA, (2005).
21. M. Dahnoun, Preparation and characterization of **Titanium** dioxide and Zinc oxide thin films via Sol-Gel (spin coating) technique for optoelectronic applications, Doctorate these, University of Biskra, 2020.
22. FENDLER, J. H. 2008. Nanoparticles and nanostructured films, Wiley. com.
23. K. L. Chopra, "Thin Film Phenomena", McGraw – Hill, New York (1969).